*Biochemical Journal* (2021) **478** 2145–2161
https://doi.org/10.1042/BCJ20210253

Research Article

# Kinetics of the multitasking high-affinity Win binding site of WDR5 in restricted and unrestricted conditions

**Ali Imran[1], Brandon S. Moyer[2], Ashley J. Canning[3], Dan Kalina[2,4], Thomas M. Duncan[3], Kelsey J. Moody[1,2,4], Aaron J. Wolfe[1,2,4], Michael S. Cosgrove[3] and Liviu Movileanu[1,5,6]**

[1]Department of Physics, Syracuse University, 201 Physics Building, Syracuse, New York 13244-1130, U.S.A.; [2]Ichor Therapeutics, Inc., 2521 US Route 11, LaFayette, New York 13084, U.S.A.; [3]Department of Biochemistry and Molecular Biology, State University of New York, Upstate Medical University, 4249 Weiskotten Hall, 766 Irving Avenue, Syracuse, New York 13210, U.S.A.; [4]Department of Chemistry, State University of New York, College of Environmental Science and Forestry, 1 Forestry Dr., Syracuse, New York 13210, U.S.A.; [5]The BioInspired Institute, Syracuse University, Syracuse, New York 13244, U.S.A.; [6]Department of Biomedical and Chemical Engineering, Syracuse University, 329 Link Hall, Syracuse, New York 13244, U.S.A.

**Correspondence:** Liviu Movileanu (lmovilea@syr.edu)

Recent advances in quantitative proteomics show that WD40 proteins play a pivotal role in numerous cellular networks. Yet, they have been fairly unexplored and their physical associations with other proteins are ambiguous. A quantitative understanding of these interactions has wide-ranging significance. WD40 repeat protein 5 (WDR5) interacts with all members of human SET1/MLL methyltransferases, which regulate methylation of the histone 3 lysine 4 (H3K4). Here, using real-time binding measurements in a high-throughput setting, we identified the kinetic fingerprint of transient associations between WDR5 and 14-residue WDR5 interaction (Win) motif peptides of each SET1 protein ($SET1_{Win}$). Our results reveal that the high-affinity WDR5-$SET1_{Win}$ interactions feature slow association kinetics. This finding is likely due to the requirement of $SET1_{Win}$ to insert into the narrow WDR5 cavity, also named the Win binding site. Furthermore, our explorations indicate fairly slow dissociation kinetics. This conclusion is in accordance with the primary role of WDR5 in maintaining the functional integrity of a large multisubunit complex, which regulates the histone methylation. Because the Win binding site is considered a key therapeutic target, the immediate outcomes of this study could form the basis for accelerated developments in medical biotechnology.

## Introduction

WD40 repeat protein 5 (WDR5) is a conserved chromatin-associated protein that is involved in a number of transient protein–protein interactions [1]. However, WDR5 is notoriously known for its regulatory role in multisubunit epigenetic complexes, such as Suppressor of Variegation, Enhancer of Zeste, and Trithorax 1 (SET1) lysine methyltransferases (KMT) of histones [2–8]. There are six SET1 family members in humans: MLL1, MLL2, MLL3, MLL4, SETd1A, and SETd1B. Each member forms a large multisubunit complex with functions that appear to have diverged in target gene localization and product specificity. However, features common among the complexes are a C-terminal catalytic SET domain that is regulated by interaction with a conserved subcomplex consisting of WDR5, retinoblastoma binding protein-5 (RbBP5), absent-small-homeotic-2-like protein (Ash2L), and dumpy-30 (DPY-30) ($WRAD_2$) [7,9–20]. WDR5 functions to bridge the interaction between the SET domain and other $WRAD_2$ subunits by the recognition of an evolutionarily conserved WDR5-interaction (Win) motif found in all SET1 family members [21–25]. Formation of this core complex is required for optimal methyltransferase activity [9,11,26]. Therefore, small molecules targeting the Win motif-WDR5 protein–protein interaction show promise as anticancer therapeutic candidates.

Received: 8 April 2021
Revised: 19 May 2021
Accepted: 21 May 2021

Accepted Manuscript online: 25 May 2021
Version of Record published: 11 June 2021

Biochemical Journal (2021) 478 2145–2161
https://doi.org/10.1042/BCJ20210253

Interestingly, recent studies have revealed that WDR5 is involved in numerous interactions with other proteins [27–29], including the transcription factor MYC oncoprotein [30–35], 3-phosphoinositide-dependent protein kinase 1 (PDPK1) [36], and interacting partners involved in phosphatidylinositol 3-kinase (PI3K) signaling [36]. Moreover, WDR5 is implicated in nongenomic activities, such as regulatory mechanisms of cellular shape, polarity, and migration [37,38]. Therefore, WDR5 is a multitasking protein with diverse roles in cellular processes [36,39,40]. Its highly conserved sequence across multiple organisms suggests the fundamental significance of its multiple roles [40].

An essential structural archetype of WDR5 is its internal cavity that hosts a high-affinity binding pocket for an evolutionarily conserved Arg-containing peptide segment of the six SET1 proteins [21–23]. Interestingly, this binding cavity of WDR5, here named the Win binding site, is the same [21,23] as that previously suggested to bind histone H3 [41–46]. Yet, the WDR5-SET1 interaction is required for the stability and functional operation of the C-terminal catalytic SET domain [11,21,22]. Moreover, it has only recently been identified that the Win binding site is implicated in transient protein–protein interactions with dozens of proteins, including those involved in PI3K signaling [36]. Given that WDR5 is overexpressed under various oncogenic conditions [47–49], the Win binding site has become a key therapeutic target for different cancers [24,25,50–59]. Therefore, a better mechanistic and quantitative understanding of the interactions of the Win binding site with other Win motif partners has fundamental and clinical significance [60–64].

Several research groups have previously examined interactions of WDR5 protein with Win-motif SET1 ($SET1_{Win}$) peptides using a variety of approaches, such as analytical ultracentrifugation (AUC) [22], isothermal titration calorimetry (ITC) [21,24,65], surface plasmon resonance (SPR) [23], and X-ray crystallography [21,23,24,65]. These explorations have confirmed the high affinity of the Win binding site for different Win motif interaction partners [24,65]. In this study, we determined the kinetic fingerprint and affinities of these interactions using high-throughput optical and fluorescence approaches, which included biolayer interferometry (BLI), SPR, and steady-state fluorescence polarization (state-state FP).

WDR5 is a 334-residue protein that has a seven-bladed, WD-40 repeat-based β propeller structure surrounding a central cavity (Figure 1A) [29,66–68]. Each blade contains four anti-parallel β strands. A segment of the central cavity serves as the high-affinity Win binding site for the $SET1_{Win}$ peptides (Figure 1B; Supplementary Figures S1, S2) [21,23,24,65]. Here, we performed a systematic kinetic analysis of the interactions of WDR5 with six 14-residue $SET1_{Win}$ peptides, which include an evolutionarily conserved Arg residue at $P_0$ (Table 1). Moreover, this Arg residue has been shown to be critical to WDR5-$SET1_{Win}$ interactions (Supplementary Table S1; Supplementary Figure S3) [22,26,69,70]. In addition, $SET1_{Win}$ sequences contain a highly conserved six-residue Win motif peptide, at positions $P_{-3}$ through $P_2$, along with eight residues on their flanking sides, at positions $P_{-7}$ through $P_{-4}$ and $P_3$ through $P_6$. These flanking residues diverge among SET1 family members, accounting for differences in the binding affinity of WDR5-$SET1_{Win}$ interactions [24,65]. The highly conserved six-residue Win motif peptide has to insert into the WDR5 binding cavity to facilitate these highly specific WDR5-$SET1_{Win}$ interactions [24,65]. Therefore, the choice of a 14-residue length of $SET1_{Win}$ was based on the requirement of the minimal six-residue Win motif sequence, along with four residues on each flanking side. This also facilitated the interpretation of our results in light of a prior crystallographic study [24], which was conducted with an identical $SET1_{Win}$ length.

Here, we employed multiple techniques to probe the effect of the surface immobilization on the kinetic fingerprint of WDR5-$SET1_{Win}$ interactions as well as to establish the efficacy of each technique for the measurement of the kinetic rate constants and binding affinities. We provide a critical analysis of each approach with respect to the kinetics of the Win binding site. BLI and SPR require surface immobilization, while steady-state FP does not. On the other hand, steady-state FP is free from this limitation, but is unable to provide real-time kinetic measurements. Furthermore, the use of multiple approaches allowed us to provide quantitative and qualitative validations of our conclusions and to obtain more generalizable outcomes that were not restrained by any one approach. Finally, we also show that distinctions in the kinetic rate constants of these interactions are correlated with unique sequences on the $SET1_{Win}$ peptides' flanking sides.

# Materials and methods

## Protein expression and purification

Human WDR5 (UniProtKB — P61964; WDR5_HUMAN) was expressed and purified, as follows. pET3aTr vectors containing the 6×His-TEV-WDR5 sequence were transformed into Rosetta™ 2 BL21(DE3)pLysS

*Biochemical Journal* (2021) **478** 2145–2161
https://doi.org/10.1042/BCJ20210253

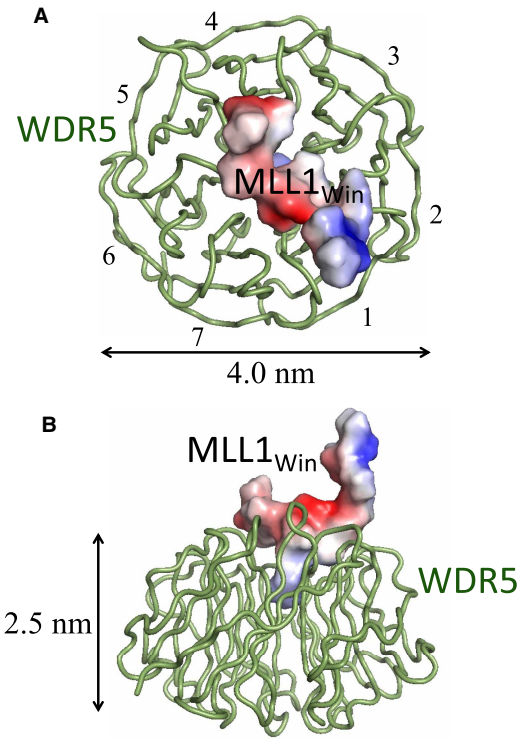


**Figure 1. Structure of the binary WDR5-MLL1$_{Win}$ complex.**
(**A**) The insertion of MLL1$_{Win}$ into the WDR5 cavity is shown from the top. (**B**) The same interaction is shown from the side. These graphic representations were made using the pdb code 4ESG [63].

(Novagen, Cat #71403) competent *E. coli* cells. Rosetta™ 2 BL21(DE3)pLysS (Novagen, Cat #71403) competent *E. coli* cells were grown overnight on Luria-Bertani (LB) agar carbenecillin/chloramphenicol selection plates at 37°C. An amount of 50 ml LB broth starter cultures (one per 10 L bioreactor growth) containing 50 μg/ml each of carbenecillin and chloramphenicol were inoculated with 5 colonies and grown for 3–5 h until turbid at 37°C. An amount of 10 L Luria broth bioreactors (Eppendorf BioFlo, Enfield, CT) containing 50 μg/ml each of carbenecillin and chloramphenicol, in addition to Antifoam 204 (Sigma–Aldrich, St. Louis, MO), were then inoculated at 37°C and 800 rpm with the entire turbid starter culture. When the culture attained $OD_{600} = 0.8$, agitation was decreased to 600 rpm and the temperature was rapidly dropped to 18°C. Induction of target proteins was initiated with 100 μM Isopropyl-β-D-1-thiogalactopyranoside (IPTG; Goldbio, St. Louis, MO) at 18°C. After 12–24 h post-induction at 18°C, cells were pelleted by centrifugation at 4465×***g*** using a J6-MI centrifuge (Beckman Coulter, Brea, CA) for 30 min at 4°C. The pellet was resuspended in 50 mM Tris–HCl (pH

**Table 1 Alignment of the amino acid sequence of SET1$_{Win}$ motifs**

| Peptide | $P_{-7}$ | $P_{-6}$ | $P_{-5}$ | $P_{-4}$ | $P_{-3}$ | $P_{-2}$ | $P_{-1}$ | $P_0$ | $P_1$ | $P_2$ | $P_3$ | $P_4$ | $P_5$ | $P_6$ | Charge |
|---|---|---|---|---|---|---|---|---|---|---|---|---|---|---|---|
| MLL1$_{Win}$: MLL1$^{3758–3771}$ | L | N | P | H | G | S | A | R | A | E | V | H | L | S[1] | 0 |
| MLL2$_{Win}$: MLL2$^{5333–5346}$ | I | N | P | T | G | C | A | R | S | E | P | K | I | L | +1 |
| MLL3$_{Win}$: MLL3$^{4703–4716}$ | V | N | P | T | G | C | A | R | S | E | P | K | M | S | +1 |
| MLL4$_{Win}$: MLL4$^{2504–2517}$ | L | N | P | H | G | A | A | R | A | E | V | Y | L | **S**[2] | 0 |
| SETd1A$_{Win}$: SETd1A$^{1488–1501}$ | E | H | Q | T | G | S | A | R | S | E | G | Y | Y | P | −1 |
| SETd1B$_{Win}$: SETd1B$^{1698–1711}$ | E | H | V | T | G | C | A | R | S | E | G | F | Y | T | −1 |

[1]This is a R3771S substituted MLL1$_{Win}$ peptide;
[2]This is a R2517S substituted MLL4$_{Win}$ peptide.

Biochemical Journal (2021) 478 2145–2161
https://doi.org/10.1042/BCJ20210253

7.4), 300 mM NaCl, 10 mM βME, and 20 mM imidazole. The resuspended cells were frozen on dry ice and stored at −80°C until purification.

Cell pellets were lysed with a Qsonica Sonicator Q700 (FisherBrand, Pittsburg, PA) on ice. An amount of 5 L of thawed, resuspended pellets were resuspended in 160 ml of 50 mM Tris–HCl (pH 7.4), 300 mM NaCl, 3 mM DTT, and 30 mM imidazole (lysis/Ni-NTA Buffer A/dialysis buffer) containing an additional 200 μl of phenylmethylsulfonyl fluoride (PMSF; Sigma–Aldrich) and two Pierce™ Protease Inhibitor Mini Tablets (EDTA-free; Thermo Fisher Scientific, Waltham, MA). The cell suspensions were stirred at 4°C for 15 min until homogeneous and then sonicated for 10 min at 90% power (2 s on, 4 s off). Lysate was then centrifuged for 1 h at 4465×***g*** and 4°C, and the supernatant was stored at 2–8°C for purification. A Ni-NTA purification process was followed. A Kontes 25 × 200 mm column with 30–40 ml Ni-NTA resin (Qiagen, Hilden, Germany) was equilibrated with at least 10 resin-bed volumes (RBVs) of 0.22 μm filtered de-ionized (DI) $H_2O$ to remove ethanol, and then at least 5 RBVs of Ni-NTA Buffer A (above). After equilibration, lysate was added to the column and washed with 5–10 RBVs of Ni-NTA Buffer A. Sample was eluted using at least 5 RBVs of Ni-NTA Buffer B (50 mM Tris–HCl (pH 7.4), 300 mM NaCl, 3 mM DTT, and 500 mM imidazole). An amount of 5 ml fractions were collected, analyzed via SDS–PAGE, and pooled. Then, sample was dialyzed, as follows. WDR5-containing fractions were pooled into 12–14 kDa MWCO dialysis tubing (Repligen, Waltham, MA), then 2.5 mg of GST-6H-TEV protease (per 5 L of culture; expressed and purified in-house) was added to cleave the His-tag, and the solution was dialyzed against 4 L of dialysis buffer (above) overnight for 12–18 h at 2–8°C. Dialyzed protein was analyzed via SDS–PAGE to ensure complete cleavage. A negative Ni-NTA was then conducted. The resulting cleaved WDR5 solution was passed through a Bio-Rad Ni-NTA IMAC cartridge (Bio-Rad, Hercules, CA) using a Bio-Rad NGC chromatography system (Bio-Rad) to remove the cleaved His-tag and GST-6H-TEV protease. The flowthrough was collected, analyzed via SDS–PAGE and UV-Vis, and concentrated for size-exclusion chromatography (SEC) purification. As a final polish, the WDR5 proteins were purified via SEC using a HiLoad® 26/600 Superdex® 200 pg column (GE Healthcare, Chicago, IL) into 20 mM Tris–HCl (pH 7.5), 300 mM NaCl, 1 μM $ZnCl_2$, 1 mM TCEP. Fractions of interest were analyzed via SDS–PAGE and UV-Vis, pooled, concentrated where necessary, aliquoted to 1 ml, flash-frozen in liquid nitrogen, and stored at −80°C.

## Peptide synthesis, labeling, purification, and analysis for BLI measurements

All peptides for biolayer interferometry measurements were synthesized by GenScript (Piscataway, NJ). The peptides were purified to ≥95% purity. Amino acid analysis, purity confirmation, and solubility testing were provided by GenScript. All peptides were biotinylated at the N terminus. Their C terminus was amidated.

## Peptide synthesis, labeling, purification, and analysis for SPR and FP measurements

For Fmoc-SPPS, peptides were synthesized at theoretical 100 μmol scale using the standard double coupling workflow pre-programmed on the Biotage Syro I peptide synthesizer (Biotage, Charlotte, NC). An amount of 278 mg of Rink Amide AM Resin LL (100–200 mesh, 0.36 mmol/g functionalization; Novabiochem (EMD Millipore)) was loaded into each 10 ml reactor vial, corresponding to the 100 μmol synthesis scale. Each resin aliquot was swelled with DMF for 30 min, followed by an initial resin deprotection step using 40% piperidine in DMF. Each double coupling cycle was comprised of two independent, 45 min coupling sub-steps that differed in the choice of activation reagents: (1) DIC/Oxyma (1 : 2 ratio with respect to Fmoc-[AA]), followed by (2) HBTU/DIPEA (0.95 : 2 ratio with respect to Fmoc-[AA]). For each coupling sub-step, four molar equivalents of each respective 0.5 M Fmoc-[AA] stock was added to each vial. Each coupling cycle terminated with a double Fmoc deprotection step using 40% piperidine in DMF. Coupling reactions proceeded with interspersed vortexing of the vials and under an air atmosphere at ambient temperature. Following the conclusion of peptide synthesis, resins were washed with three successive aliquots of DCM, followed by 3 min under vacuum to dry.

Each peptidyl-resin aliquot was swelled with DMF for 30 min and drained. DMF (1200 μl) was added to each aliquot, followed by 300 μl of DIPEA in NMP (six molar equivalents, 600 μmol), then followed by 600 μl of Lissamine Rhodamine B sulfonyl chloride in DMF (three molar equivalents, 300 μmol). The mixture was shielded from light and allowed to react with intermittent vortexing overnight at ambient temperature. Following conjugation, the resin bed was drained, washed successively with DMF until no further change in the

color of the flowthrough was observed (faint pink), washed successively with DCM, and then held under vacuum for 3 min to dry.

Cleavage cocktail containing 90% TFA, 5% TIS, 2.5% DODT, and 2.5% $H_2O$ was freshly prepared. An amount of 4 ml of cleavage cocktail was added to each peptidyl-resin aliquot, sealed, and placed on a rocking platform to react for 4 h at ambient temperature. After incubation, the contents of each reactor vial were plunged into separate 50 ml conical tubes. The resin was then treated with an additional 2 ml of cleavage cocktail and allowed to react on the rocking platform for 30 min at ambient temperature. Following the second incubation, the contents of each reactor vial were pooled into their respective 50 ml conical tubes and the resin containing reactor vials were discarded. Cleavage aliquots were triturated by the fast addition of ∼45 ml cold (−80°C) diethyl ether. Precipitate was compacted by centrifugation at 1000×***g*** for 10 minutes at 0°C using an Allegra X-22R centrifuge (Beckman Coulter, Brea, CA). The supernatant was discarded, and the peptide pellets were washed with a second ∼30 ml aliquot of cold diethyl ether, centrifuged, and decanted as before. The resulting peptide pellets were flash frozen in liquid nitrogen and lyophilized using a FreeZone 2.5L lyophilizer (Labcono, Kansas City, MO) overnight to remove residual solvents. The crude lyophilized peptide was stored at −80°C until purification.

Crude peptide aliquots were purified using reversed-phase chromatography through two stages: (1) Flash chromatography using a Biotage Isolera One (Biotage AB, Uppsala, Sweden), (2) Semi-preparative HPLC using a Waters 2695 separations module equipped with a Waters 2996 photodiode array detector (PDA). (1) Biotage Isolera One purifications: Each crude peptide aliquot was solubilized in 2.5 ml total of either DMSO or DMF (DMF only if the peptide contained oxidizable Cys or Met residues) and loaded onto a Biotage Sfär $C_{18}$ Samplet for 25 g Column (Biotage, Uppsala, Sweden) with the aid of a vacuum. Each samplet was placed in a Biotage Sfär Bio $C_{18}$ D Duo (300 Å, 20 μm) 25 g column (Biotage). Peptides were eluted using a 15-column volume (CV) gradient of 9–90% MeCN in $H_2O$ containing 0.1% TFA at a flowrate of 30 ml/min. The collection threshold was 75 mAU for $\lambda = 200–400$ nm, with monitoring at $\lambda = 215$ nm and 355 nm (rhodamine). Rhodamine labeled fractions were pooled and MeCN was removed using a rotary evaporator for 30 min at 25° C. Samples were flash-frozen in liquid nitrogen and lyophilized using a FreeZone 2.5L lyophilizer (Labcono) for 3 days. The semi-pure lyophilized peptide was stored at −80°C until further purification. (2) Semi-preparative HPLC: Peptide samples were resuspended in 50–80 μl aliquots of DMSO or 1 : 2 DMSO/$H_2O$. Aliquots were injected onto a Waters XBridge Peptide BEH $C_{18}$ OBD Prep Column (5 μm, 300 Å, 10 mm × 150 mm). A gradient of 10–50% MeCN containing 0.1% (v/v) TFA in $H_2O$ containing 0.1% (v/v) TFA was applied over 40 min (Δ1%/min.) at a flow rate of 4.73 ml/min. at ambient temperature using a Waters 2695 separations module. Sample detection occurred at 215 nm, 280 nm, 355 nm (rhodamine), and 560 nm (rhodamine) using a Waters 2996 photodiode array detector (PDA). Sample purity was determined by baseline integration using Waters Empower 3 software (>90% purity in all cases). Rhodamine containing fractions were analyzed by MALDI-TOF mass spectroscopy for the identity and purity confirmatory tests. Target fractions were flash-frozen in liquid nitrogen and lyophilized using a FreeZone 2.5L lyophilizer (Labcono) for three days. The resulting purified, lyophilized peptides were reconstituted as concentrated stocks in ultrapure water, aliquoted, flash-frozen in liquid nitrogen, and stored at −80°C until use.

For MALDI-TOF mass spectroscopy of the purified peptides, 1 μl of peptide stock in $H_2O$ (1–100 μM) was mixed with 9 μl spotting matrix (10 mg/ml α-cyano-4-hydroxycinnamic acid (CHCA) in 50 : 50 MeCN/0.1% (v/v) TFA in $H_2O$). An amount of 2 μl of each peptide spotting solution was spotted onto a Bruker MTP 384 Target Plate, which was calibrated using Anaspec Peptide Mass Standard Kit, and allowed to dry at room temperature for at least 30 min prior to analysis. Samples were analyzed on a Bruker Autoflex iii Mass Spectrometer as an average of 1200 shots using 35% laser power, an $m/z$ range from 840–6000 Da with suppression <400 Da in linear mode, 3.6× detector gain, 2.00 sample rate, and medium gating strength.

## Biolayer interferometry (BLI)

Octet RED384 (FortéBio, Fremont, CA) was used for the BLI studies [71–73]. Streptavidin (SA) sensors were presoaked in buffer for ∼30 min. The buffer solution contained 150 mM NaCl, 20 mM Tris–HCl, 1 mM TCEP, 1 mg/ml bovine serum albumin (BSA), pH 7.5. An amount of 5 nM tagged peptide was then loaded onto sensors for 15 min. Sensors were then dipped in buffer again for 5 min to wash off unbound peptides from the surface. A 3-fold serial dilution of WDR5 was conducted ranging from 0.1 μM to 9 μM for the association process and then placed into the buffer solution for the dissociation process. The association and dissociation processes were ∼200 and ∼600 s long, respectively. For all WDR5 concentrations, unloaded sensors were run

Biochemical Journal (2021) 478 2145–2161
https://doi.org/10.1042/BCJ20210253

concurrently as controls and were used to subtract the baseline and the drift in the sensorgrams to extract the binding curves. The BLI experiments were performed at 24°C. All reagents were prepared in the above- mentioned buffer and were loaded into 96-well flat bottom black plates for the sensorgram recordings. The binding curves were fitted using the Octet Data Analysis software (FortéBio). The curves of the association process, which were recorded for various analyte concentrations, [$C$], were fitted using the following equation [74]:

$$Y = Y_\infty - (Y_\infty - Y_0)e^{-k_{obs}t} \quad (1)$$

Here, $Y_0$ and $Y_\infty$ are the BLI response signals at time zero and infinity, respectively, of the association process. $t$ denotes the cumulative time of the association reaction. $k_{obs}$ is the apparent first-order reaction rate constant of the association process. The curves of the dissociation process were fitted using the following equation:

$$Y = Y_\infty + (Y_0 - Y)e^{-k_{off}t} \quad (2)$$

Here, $Y_0$ and $Y_\infty$ are the BLI response signals at time zero and infinity, respectively, of the dissociation process. $k_{off}$ indicates the dissociation rate constant. Finally, the association rate constant, $k_{on}$, was determined using the slope of the linear curve [75,76]:

$$k_{obs} = k_{on}[C] + k_{off} \quad (3)$$

Global fitting, which was conducted using several analyte concentrations, provided the corresponding $k_{on}$ and $k_{off}$ values. The dissociation constant, $K_D$, were indirectly determined using the $k_{on}$ and $k_{off}$ values. Three distinct BLI measurements were conducted for all inspected interactions.

## Surface plasmon resonance (SPR)

All SPR experiments [77–79] were conducted on a Cytiva Biacore 8K (Cytiva Life Sciences, Marlborough, MA). All buffers and dilutions were freshly made in-house using ultrapure water obtained from an IQ 7000 Milli-Q system (Millipore-Sigma, Burlington, MA). WDR5 protein was immobilized onto the active flow cell of each channel of a Cytiva Series S Sensor Chip CM5 (Cytiva Life Sciences) according to the following parameters and protocol. A CM5 chip was inserted into the instrument and equilibrated for 1 h at 25°C in PBS-P+ running buffer (PBS-P+ Buffer 10×, Cytiva Life Sciences). The chip surface was activated using an injection of 1 : 1 N- hydroxysuccinimide (NHS)/1-ethyl-3-(3-dimethylaminopropyl)carbodiimide (EDC) (Cytiva Amine Coupling Kit, Cytiva Life Sciences) for 420 s at 10 μl/min across both active and reference flow cells. This activation process was followed by a wash of the microfluidics with 1 M ethanolamine-HCl (pH 8). Following activation, wild-type WDR5 (1.75–2.50 μg/ml; analyte dependent) in 50 mM sodium phosphate (pH 6.5), 50 mM NaCl was then injected across the active flow cell for 150 s at 10 μl/min. Following ligand immobilization, both active and passive flow cells were chemically deactivated with an injection of 1 M ethanolamine-HCl (pH 8) for 420 s at 10 μl/min. $SET1_{Win}$ peptide dilutions were freshly prepared from HPLC- purified peptide stocks in ultrapure water; the peptides were identical with those used in the steady-state FP experiments and contained an N-terminal sulforhodamine B and a C-terminal amide. Titrations of each labeled $SET1_{Win}$ peptide analyte were conducted to span an approximate range of $0.1–10 \times K_D$ (~1 nM to 7 μM; 40 μM for MLL1). Each $SET1_{Win}$ peptide was analyzed in a separate channel. Multicycle kinetic analyses were conducted at a flow cell temperature of 25°C and a sample compartment temperature of 20°C in a running buffer composed of 20 mM Tris- HCl (pH 7.5), 150 mM NaCl, 1 mM TCEP, 0.05% Tween 20. Each analysis cycle consisted of the following steps: (1) $SET1_{Win}$ peptide analyte injection: 120 s association, 360 s dissociation, 30 μl/min.; (2) regeneration injection with 100% ethylene glycol for 15 s at 10 μl/min. (high viscosity setting); (3) wash of the microfluidics system with running buffer; (4) regeneration injection with 1 μM $ZnCl_2$ for 30 s at 10 μl/min. Prior to curve fitting, all data generated from the active flow cell of each channel are double referenced to both the appropriate buffer blanks (first/last) and the reference flow cell. For $MLL2_{Win}$, $MLL3_{Win}$, $MLL4_{Win}$, $SETd1A_{Win}$, and $SETd1B_{Win}$, the affinity constants, $K_D$, were calculated indirectly using $K_D = k_{off}/k_{on}$. For $MLL1_{Win}$, a plot of relative response versus the $MLL1_{Win}$ analyte concentration was constructed and data were fitted using a four-parameter logistic regression to obtain the $K_D$. Therefore, an affinity analysis (relative response vs. concentration dose- response curve) was used to calculate the $K_D$, in this instance due to kinetic

rate constants falling outside of the instrument detection range. All interactions were independently determined in triplicate (e.g. separate ligand immobilizations). Experimental data and fits were plotted using GraphPad Prism 8 (GraphPad Software).

### Steady-state fluorescence polarization (steady-state FP) measurements

All steady-state fluorescence polarization (FP) measurements were recorded using a SpectraMax i3x plate reader (Molecular Devices, San Jose, CA).[80,81] HPLC-purified peptides, which contained an N-terminal sulforhodamine B and a C-terminal amide, were reconstituted as concentrated stocks in ultrapure water and used in all subsequent experiments. All steady-state FP assays were conducted in a buffer containing 20 mM Tris–HCl (pH 7.5), 150 mM NaCl, 1 mM TCEP, 0.005% Tween 20 and plated in black untreated 96-well polystyrene microplates (Corning Inc., Corning, NY). Steady-state FP assays were conducted in triplicate, 24-point serial dilution for each of the six SET1Win peptides against WDR5. An amount of 200 μl of WDR5 stock solutions, ranged from 21.6 to 131 μM, were added to each well on the first column of one of two adjacent black 96-well dilution plates, and 100 μl of the assay buffer was added to wells A2-H24 over the two plates. WDR5 variants were then diluted down the two plates by transferring 100 μl from each well to the next, for a total of 24, 2-fold dilutions which range from low μM to low pM (variant specific). Following dilutions, 100 μl of the appropriate 20 nM labeled $SET1_{Win}$ peptide, which was dissolved in the assay buffer, was added to each well on each set of plates at a final concentration of 10 nM. The steady-state FP anisotropy was measured on the plates after a 1 h incubation at room temperature in the dark. The resulting dose-response data were averaged and fitted using a four-parameter logistic regression to obtain the binding affinity ($K_D$) for each interaction. Data were plotted and analyzed using GraphPad Prism 8 (GraphPad Software, San Diego, CA).

### Molecular graphics

All cartoons showing molecular graphics were prepared using the PyMOL Molecular Graphics System (Version 2.4.0 Schrödinger, LLC).

## Results and discussion

### The kinetic fingerprint of WDR5 — $SET1_{Win}$ interactions

We first explored the association ($k_{on}$) and dissociation ($k_{off}$) rate constants of WDR5-$SET1_{Win}$ interactions using BLI measurements [71,72]. This technology probes ligand-receptor interactions that lead to accumulations of bimolecular complexes at the surface of the BLI sensor. This process is facilitated by immobilizing one interacting partner (ligand) onto the surface of the BLI sensor and supplying the analyte partner (receptor) from solution. In this way, the association and dissociation phases of the ligand-receptor complex are optically measured in real time using alterations in the interference pattern between reflected light waves at the surface of the BLI sensor. The N-terminus of each $SET1_{Win}$ was biotinylated and their C-terminus was amidated (Table 1). A nine- residue Gly/Ser-rich peptide spacer was inserted between the biotinylated site and the $SET1_{Win}$ sequence. This 3 nm-long spacer ensures that there is a satisfactory distance between the BLI sensor and $SET1_{Win}$ for WDR5 to interact without steric hinderance from the sensor surface.

The association binding curves were acquired through a 3-fold serial dilution of WDR5 (Figure 2). After the BLI response reached a saturation level, individual dissociation binding curves were recorded when sensors were placed in a WDR5-free buffer. The association and dissociation BLI phases underwent a time-dependent single-exponential increase and decrease, respectively. The binding curves were fitted using the Octet Data Analysis software (Materials and Methods; eqns. (1)–(3)). The equilibrium dissociation constants using BLI, $K_{D\text{-}BLI}$, were indirectly determined using $k_{on}$ and $k_{off}$.

#### Association rate constants

The BLI-determined $k_{on}$ values were in the order of $10^4$ $M^{-1}$ $s^{-1}$, clearly indicating slow association kinetics for a protein–peptide system (Table 2). It is likely that this outcome resulted from two distinct physical restrictions: (i) tethering $SET1_{Win}$ onto the surface of the BLI sensor, thus reducing its local mobility, and (ii) partitioning of $SET1_{Win}$ into the WDR5 cavity. The latter physical process was illustrated in early crystallographic studies [21], which revealed that an $MLL1_{Win}$ peptide penetrates into the WDR5 cavity to undergo a bimolecular association process. Here, we were unable to acquire an accurate mean value of $k_{on}$ for the WDR5-$MLL1_{Win}$ interaction due to its relatively fast $k_{off}$ constant, whose binding time constant was shorter than the time-resolution

*Biochemical Journal* (2021) **478** 2145–2161
https://doi.org/10.1042/BCJ20210253

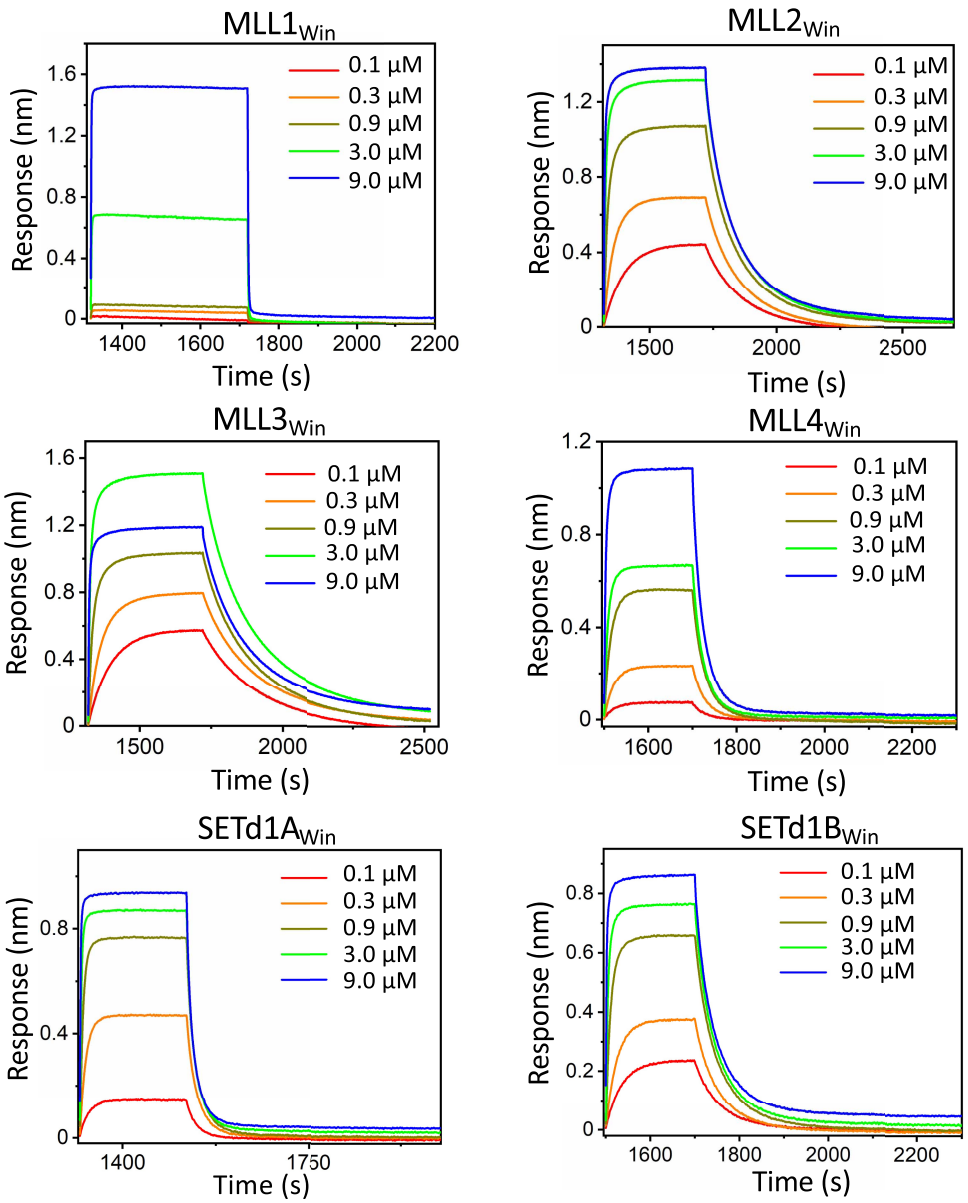


**Figure 2. Label-free optical BLI sensorgrams of WDR5-SET1$_{Win}$ interactions.**

5 nM biotin-tagged SET1$_{Win}$ peptides were loaded onto streptavidin (SA) sensors for 15 min. Titration series of WDR5 were injected as analytes and the corresponding association and dissociation curves are shown for the six SET1$_{Win}$ peptides.

limit of this approach (~1 s). Furthermore, $k_{on}$ measured by BLI for various SET1$_{Win}$ peptides were within the same order of magnitude, suggesting a similar insertion mechanism of the six-residue Win motif peptide into the Win binding site (Table 1; Supplementary Figures S1, S2) [24,65].

## Dissociation rate constants

In contrast, $k_{off}$ values spanned between two and three orders of magnitude (Table 2), highlighting significant distinctions in the WDR5-SET1$_{Win}$ interactions. This assumes that the $k_{off}$ of the WDR5-MLL1 interactions is faster than 1 $s^{-1}$, showing that MLL1$_{Win}$ has the weakest interaction with WDR5 among all SET1$_{Win}$ peptides. On the other hand, the strongest WDR5-SET1$_{Win}$ interactions were monitored with MLL2$_{Win}$ and MLL3$_{Win}$, which had average $k_{off}$ values of $(7.7 \pm 0.2) \times 10^{-3}$ $s^{-1}$ and $(5.3 \pm 0.1) \times 10^{-3}$ $s^{-1}$, respectively. This finding provides unusually long binding times of ~130 s and ~190 s, respectively.

**Table 2 Kinetic rate constants of association, $k_{on}$, and dissociation, $k_{off}$, and equilibrium dissociation constants, $K_{D\text{-}BLI}$, of WDR5 with $SET1_{Win}$ peptides using BLI**

| Peptide sequence | $k_{on}$ ($M^{-1}$ $s^{-1}$) × $10^{-4}$ | $k_{off}$ ($s^{-1}$) × $10^{3}$ | $K_{D\text{-}BLI}$ (nM) |
|---|---|---|---|
| Biotinyl-$(GGS)_3MLL1_{Win\text{-}NH2}$ | ND[1] | ND[2] | ND[3] |
| Biotinyl-$(GGS)_3MLL2_{Win\text{-}NH2}$ | 4.4 ± 0.4 | 7.7 ± 0.2 | 170 ± 20 |
| Biotinyl-$(GGS)_3MLL3_{Win\text{-}NH2}$ | 5.4 ± 0.6 | 5.3 ± 0.1 | 100 ± 5 |
| Biotinyl-$(GGS)_3MLL4_{Win\text{-}NH2}$ | 2.3 ± 0.2 | 39 ± 2 | 1700 ± 200 |
| Biotinyl-$(GGS)_3SETd1A_{Win\text{-}NH2}$ | 8.2 ± 0.8 | 51 ± 6 | 620 ± 20 |
| Biotinyl-$(GGS)_3SETd1B_{Win\text{-}NH2}$ | 7.1 ± 0.5 | 17 ± 1 | 250 ± 30 |

[1] $k_{on}$ was not quantitatively determined. Although WDR5-$MLL1_{Win}$ interactions were detectable using a BLI measurement (Figure 2), no accurate quantitative determination was made due to the limited time resolution of this approach. In this case, we assume that the $k_{on}$ was in the same order of magnitude with the $k_{on}$ of the other $SET1_{Win}$ peptides (~$10^4$ $M^{-1}$ $s^{-1}$);
[2] $k_{off}$ was not quantitatively determined due to a fast dissociation rate constant. The upper- limit value for the detection of $k_{off}$ is 1 $s^{-1}$ according to instrument specifications;
[3] $K_{D\text{-}BLI}$ was not quantitatively determined due to the limited time resolution of the approach. In this case, $K_{D\text{-}BLI}$ determined by BLI for WDR5-$MLL1_{Win}$ interactions should be greater than ~$10^5$ nM. This value results from dividing the upper-limit value of detection of $k_{off}$ (ND**) by the value of the $k_{on}$ approximation (ND*);Numbers represent mean ± s.d. determined from three independent experiments.

It was previously demonstrated that WDR5-$SET1_{Win}$ interactions have a common archetype: a highly conserved Arg residue at $P_0$ (Table 1) [22]. This Arg residue is the pivotal player of WDR5-$SET1_{Win}$ interactions, contributing to most of the binding affinity through a complex network of contacts with neighboring residues (Supplementary Table S1; Supplementary Figure S3) [22,24]. To test this hypothesis, we conducted BLI measurements using a control $MLL3_{Win}$ peptide, whose native form exhibited the longest binding time with WDR5. The key Arg residue at $P_0$ was replaced by an Ala residue, resulting in the R4710A $MLL3_{Win}$ mutant. No interaction was detected with this R4710A $MLL3_{Win}$ mutant (Supplementary Figure S4), confirming the critical role of Arg at $P_0$ for the strength of WDR5-$SET1_{Win}$ interactions. In addition, this finding validates the efficacy of our BLI measurements for examining the kinetic landscape of the Win binding site of WDR5.

## Does the tethering restriction of $SET1_{Win}$ onto the surface of the BLI sensor impact the kinetic rate constants?

### Association rate constants

We postulated above that the slow association kinetics of WDR5-$SET1_{Win}$ interactions were caused at least in part by the immobilization of $SET1_{Win}$ onto the surface of the BLI sensor. To assess this hypothesis, we next employed SPR [77–79] as an orthogonal, label-free approach for examining these interactions of $SET1_{Win}$ peptides with WDR5. SPR is an optoelectronic technique that monitors accumulation of bimolecular ligand-receptor complexes onto the surface of the SPR sensor by changes in the refractive index. In this case, $SET1_{Win}$ analyte is supplied by using a flow-driven fluidic device. WDR5 was immobilized onto the surface of the SPR chips as the 'receptor' (Materials and Methods). In this way, we recorded the association and dissociation phases in real time when $SET1_{Win}$ was not immobilized onto a surface (Figure 3). Biacore™ Software was used to analyze and fit the SPR sensorgrams using a 1 : 1 binding interaction model to provide the $k_{on}$ and $k_{off}$ rate constants (Supplementary Figure S5). In accord with our expectation, $k_{on}$ values obtained by SPR were significantly increased by almost an order of magnitude to quantities greater than $10^5$ $M^{-1}$ $s^{-1}$ (Table 3; Supplementary Figures S6, S7A). Again, $k_{on}$ measured by SPR for various $SET1_{Win}$ peptides were within the same order of magnitude, potentially indicating an identical insertion mechanism of the six-residue Win motif peptide into the Win binding site (Table 1; Supplementary Figures S1, S2) [24,65]. In addition, this insertion mechanism prevails no matter whether $SET1_{Win}$ is in either physically restricted (e.g. BLI) or unrestricted (e.g. SPR) conditions.

### Dissociation rate constants

Interestingly, with the exception of SETd1A, the $k_{off}$ values acquired by the SPR measurement of WDR5-$SET1_{Win}$ interactions closely resembled those measured by BLI (Table 3; Supplementary Figure S7B).

*Biochemical Journal* (2021) **478** 2145–2161
https://doi.org/10.1042/BCJ20210253

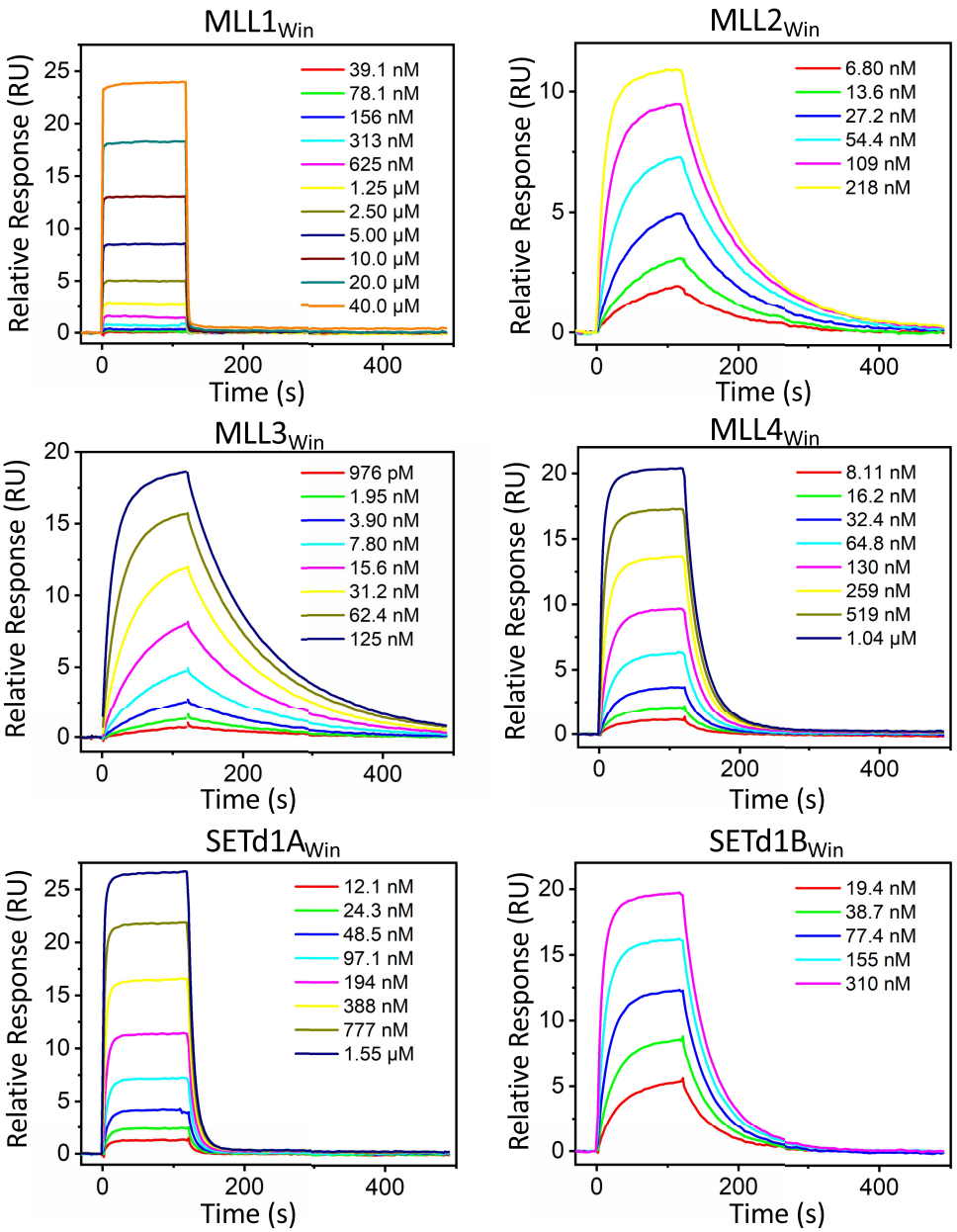


**Figure 3. Label-free optoelectronic SPR sensorgrams of the WDR5-SET1$_{Win}$ interactions.**

Titration series of the respective SET1$_{Win}$ peptides were injected as analytes and the corresponding association and dissociation curves are shown for the six SET1$_{Win}$ peptides.

Moreover, this finding provides indirect evidence that WDR5 did not undergo denaturation upon its immobilization onto the surface of the SPR sensor. Tethering SET1$_{Win}$ onto the surface of the BLI sensor via its C-terminus was considered inconvenient, because prior crystallographic information indicated the interaction of the C-terminus residues (Table 1) with the WDR5 surface [24]. However, does the SET1$_{Win}$ tethering onto the surface of the BLI sensor via its N-terminus impose an additional physical restriction on the binding mechanism? Since the $k_{off}$ measured by BLI and SPR are almost identical, we conclude that the SET1$_{Win}$ tethering onto the surface of the BLI sensor via its N-terminus did not produce any additional restrain on the detachment mechanism of SET1$_{Win}$ from the high-affinity Win binding site.

*Biochemical Journal* (2021) **478** 2145–2161
https://doi.org/10.1042/BCJ20210253

**Table 3 Kinetic and affinity determinations of WDR5-SET1$_{Win}$ interactions using SPR**

| Peptide sequence | $k_{on}$ ($M^{-1}$ $s^{-1}$) × $10^{-5}$ | $k_{off}$ ($s^{-1}$) × $10^{3}$ | $K_{D\text{-}SPR}$ (nM) |
|---|---|---|---|
| Sulforhodamine B-$(GGS)_3$MLL1$_{Win\text{-}NH2}$ | ND[1] | ND[2] | 16 000 ± 3000[3] |
| Sulforhodamine B-$(GGS)_3$MLL2$_{Win\text{-}NH2}$ | 3.7 ± 0.3 | 12 ± 1 | 33 ± 2 |
| Sulforhodamine B-$(GGS)_3$MLL3$_{Win\text{-}NH2}$ | 4.9 ± 0.4 | 9 ± 1 | 19 ± 1 |
| Sulforhodamine B-$(GGS)_3$MLL4$_{Win\text{-}NH2}$ | 2.1 ± 0.3 | 41 ± 3 | 190 ± 20 |
| Sulforhodamine B-$(GGS)_3$SETd1A$_{Win\text{-}NH2}$ | 3.1 ± 0.2 | 110 ± 10 | 350 ± 10 |
| Sulforhodamine B-$(GGS)_3$SET1dB$_{Win\text{-}NH2}$ | 3.4 ± 0.3 | 24 ± 1 | 69 ± 6 |

[1]$k_{on}$ was not quantitatively determined. Although the WDR5-MLL1$_{Win}$ interactions were detectable using an SPR measurement (Figure 3), no accurate quantitative determination was made due to the limited time resolution of the approach. In this case, we assume that the $k_{on}$ was in the same order of magnitude with the $k_{on}$ of other SET1$_{Win}$ peptides (~$10^5$ $M^{-1}$ $s^{-1}$);
[2]$k_{off}$ was not quantitatively determined due to a fast dissociation rate constant. The upper-limit value for the detection of $k_{off}$ is 0.5 $s^{-1}$ according to instrument specifications. The Biacore 8K+ cannot measure rate constants of dissociation, $k_{off}$, faster than 0.5 $s^{-1}$;
[3]Here, $K_{D\text{-}SPR}$ was determined using a steady-state SPR measurement (Supplementary Figure S6);
Values represent mean ± s.d. acquired from at least three independent experimental determinations (separate receptor immobilizations).
For MLL2$_{Win}$, $n = 4$ independent experimental determinations were used.

## Comparisons of binding affinities of WDR5-SET1$_{Win}$ interactions in restricted and unrestricted conditions

Next, we asked how immobilization-free (i.e. unrestricted) conditions influence the binding affinities. It is expected that the equilibrium dissociation constant slightly decreases if both WDR5 and SET1$_{Win}$ move freely in solution. Hence, we determined equilibrium dissociation constant values using steady-state FP measurements, $K_{D\text{-}FP}$ (Materials and Methods) [80–82]. This fluorescence technique monitors changes in the polarity of the emitted light due to modifications in the rotational diffusion coefficient of a fluorescently labeled ligand. For example, the formation of the ligand-receptor complex is accompanied by a decline in the rotational mobility of the ligand, increasing the polarity of the emitted light. Here, Sulforhodamine B, an optically stable and bright fluorophore [83], was chemically attached to the N terminus of SET1$_{Win}$ via a nine-residue Gly/Ser-rich flexible spacer, whereas their C terminus was amidated. WDR5 concentration-dependent, steady-state FP binding curves were collected using a plate reader in a high-throughput setting (Figure 4). In this way, we determined the immobilization-free $K_{D\text{-}FP}$ (Supplementary Table S2). In accord with our anticipation, $K_{D\text{-}FP}$ values were slightly lower than those acquired by SPR, $K_{D\text{-}SPR}$, meaning that WDR5-SET1$_{Win}$ interactions appeared somewhat stronger when probed in unrestricted conditions.

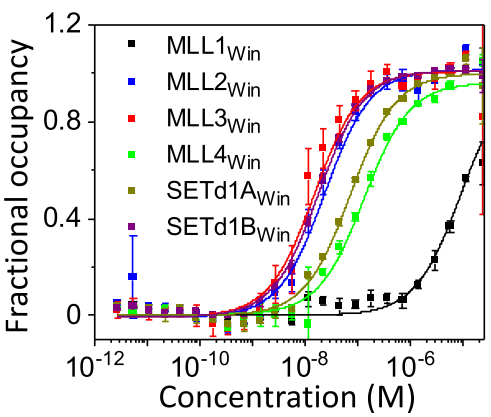


**Figure 4. Steady-state FP curves of the WDR5-SET1$_{Win}$ interactions.**
The N terminus of the SET1$_{Win}$ peptides was tagged with sulforhodamine B, whereas the C terminus was amidated. The final concentration of labeled SET1$_{Win}$ peptides in each well was 10 nM. Three independent experiments were conducted to obtain the WDR5 dose response.

*Biochemical Journal* (2021) **478** 2145–2161
https://doi.org/10.1042/BCJ20210253

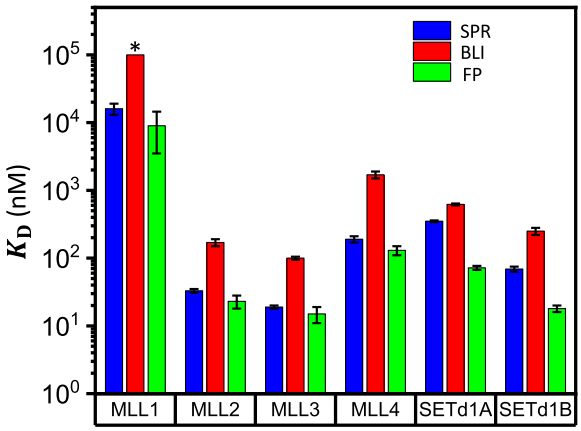


**Figure 5. Quantitative comparisons of dissociation equilibrium constants of WDR5-SET1$_{Win}$ interactions using BLI, SPR, and steady-state FP measurements.**

'*' is the upper- limit value for the detection of $K_{D\text{-}BLI}$. This value results from dividing the upper-limit value of the detection of $k_{off}$ by the value of the $k_{on}$ approximation (Table 2).

The $K_{D\text{-}FP}$ values are also in agreement with results of prior ITC measurements (e.g. in immobilization-free conditions) at either lower [65] or higher salt concentrations [24]. It is worth mentioning that we preferred replacing Arg by Ser at the C terminus of MLL1$_{Win}$ and MLL4$_{Win}$ to avoid potential rebinding events of the native Arg at $P_6$ to the WDR5 cavity (Table 1). Regardless, we employed similar peptide sequences and identical buffer conditions to obtain meaningful comparisons among the three approaches. Then, we have discovered the following relationship for each WDR5-SET1$_{Win}$ interaction: $K_{D\text{-}BLI} > K_{D\text{-}SPR} > K_{D\text{-}FP}$ (Figure 5; Supplementary Table S2). In addition, numerical values of $K_{D\text{-}FP}$ replicated similar trends noted with different SET1$_{Win}$ peptides using both BLI and SPR.

## Tentative interpretations

The kinetics and affinity measurements of the WDR5-SET1$_{Win}$ interactions were conducted with no significant variation among independently recorded BLI sensorgrams. The precision of this technique allowed us to quantitatively compare kinetics that were within the same order of magnitude. The SET1$_{Win}$ motif is located ~60 residues N-terminal to the SET domain, both of which are at the C-terminal end of the large SET1 proteins. These proteins range between ~1700–5500 amino acids in length. The rotational and diffusional rates of SET1 proteins relative to WDR5 are slow enough that these proteins can be considered as stationary compared with WDR5. Therefore, a more physiologically-relevant approach that recapitulates the binding of the full-length SET1 is that in which the 14-residue SET1$_{Win}$ peptide is attached onto a surface, whereas WDR5 is free in solution. In this way, the actual $k_{on}$ measured by BLI would be conceivably closer to that value in physiological conditions. In addition, it should be mentioned that SET1$_{Win}$ is physically restrained at both ends when it is part of the SET1 subunit, suggesting an even lower $k_{on}$ value. However, SET1$_{Win}$ may have stabilized conformations that promote binding within the context of the large SET1 subunit. In other words, the unrestricted SET1$_{Win}$ may undergo significantly greater degrees of freedom to adopt numerous non-productive conformations. Furthermore, binding of SET1 proteins to WDR5 may be coupled with additional interaction pockets that can amplify the binding strength either by increasing $k_{on}$ or by decreasing $k_{off}$ or both. For example, prior sedimentation velocity experiments have shown that a 225-residue MLL1$_{Win}$-containing polypeptide exhibits a binding affinity of ~120 nM to WDR5 [22].

$k_{on}$ values measured by SPR are yet at least an order of magnitude lower than those predicted for a protein–peptide interaction system ($10^7$–$10^8$ $M^{-1}$ $s^{-1}$) [84–88]. Here, WDR5-SET1$_{Win}$ interactions require a precise insertion of the six-residue, Arg-containing SET1$_{Win}$ peptide into the WDR5 cavity. Therefore, we interpret that $k_{on}$ values are limited by the entropic penalty determined by the SET1$_{Win}$ partitioning into the Win binding site. The high-affinity Win binding site features a conical geometry with a maximum internal diameter of ~1.5 nm, as measured from side chain to side chain. For example, MLL1$_{Win}$ partitions ~1.0 nm into the

Win binding site (Figure 1) [24]. In support to this interpretation, previous single-molecule studies have shown that $k_{on}$ values of the interactions of peptides, up to 25 residues in length, with a narrow 2 nm-wide nanopore are in the order of $10^5$ $M^{-1}$ $s^{-1}$ [89,90]. This is the same order of magnitude with $k_{on}$ values that we determined by SPR.

However, the $k_{on}$ is a composite parameter, which includes contributions of the diffusion-limited rate factor, $k_{on0}$, and electrostatic free energy of the WDR5-$SET1_{Win}$ complex, $\Delta G^{\star}_{el}$. Zhou and coworkers have demonstrated that the rate constant of association of two proteins can be accurately computed using the following expression: $k_{on} = k_{on0} \exp(-\Delta G^{\star}_{el}/k_B T)$, where $k_B$ and $T$ are Boltzmann's constant and the absolute temperature, respectively [91,92]. For this equation, they employed kinetic-rate theory of rigid-body docking and Poisson-Boltzmann formalism [93–95]. Using the same approach [93] and crystallographic information of the WDR5-$SET1_{Win}$ complex [24], we found $k_{on}$ values of several $SET1_{Win}$ peptides (Supplementary Table S3). For example, computed $k_{on}$ values for $MLL2_{Win}$ and $MLL3_{Win}$ were $2.9 \times 10^5$ $M^{-1}$ $s^{-1}$ and $1.2 \times 10^5$ $M^{-1}$ $s^{-1}$, respectively. These values compare well with our corresponding experimental data determined by SPR, which were $(3.7 \pm 0.3) \times 10^5$ $M^{-1}$ $s^{-1}$ and $(4.9 \pm 0.4) \times 10^5$ $M^{-1}$ $s^{-1}$, respectively. Yet, computed $k_{on}$ values for $MLL1_{Win}$ and $MLL4_{Win}$ were in the order of $10^4$ $M^{-1}$ $s^{-1}$. The TransComp server: Web Server for Predicting Protein Association Rate Constants [91,93] was not able to produce computed $k_{on}$ values for $SETd1A_{Win}$ and $SETd1B_{Win}$, likely because these WDR5-$SET1_{Win}$ complex formations do not undergo a single-step association mechanism. This outcome suggests that the WDR5-$SET1_{Win}$ interactions of $SETd1A_{Win}$ and $SETd1B_{Win}$ exhibit some subtle structural distinctions with respect to $MLL1_{Win}$, $MLL2_{Win}$, $MLL3_{Win}$, and $MLL4_{Win}$, which is in accord with prior crystallographic data [24,65].

## Concluding remarks, practical implications, and future prospects

In summary, we present a detailed kinetic fingerprint of the multitasking high-affinity Win binding site of WDR5, a protein with major regulatory implications in the methylation of H3K4 and in multiple physical associations with other proteins. This study reveals slow kinetics of association and dissociation of the $SET1_{Win}$ peptides with WDR5. It is known that WDR5 bridges the interaction between the SET domain of large SET1 subunits and other $WRAD_2$ constituents. A long-binding time of WDR5-$SET1_{Win}$ interaction, meaning slow dissociation kinetics of the high-affinity Win binding site, is a pivotal mechanism by which WDR5 assists the functional integrity of the multisubunit $WRAD_2$ complex. Furthermore, slow dissociation rates detected in this study point out a fundamental consideration for future therapeutics aimed at targeting interactions of the Win binding site with other proteins. The stability of these multisubunit complexes would decrease the opportunities for inhibitors to interfere in WDR5-SET1/MLL interactions. Consequently, this stresses the need for both fast association rates and slow dissociation rates when designing potential inhibitors to modulate WDR5 function. Newly designed small-molecule drugs would need to bind strongly to the WDR5 cavity and stave off other binding partners. Slow dissociation rate constants also reiterate the efficacy of $SET1_{win}$ peptidomimetics as a fundamental platform for such drugs. Modifications of these sequences that enhance the association rates, while maintaining the disassociation rates, could be very effective at inhibiting Win binding site interactions. A good place to start would be the alteration of either the net charge or charge distribution of these peptides for amplifying the rate constants of association. Any approach employed in this work can be used in the high-throughput screening of libraries of small-molecule compounds against WDR5-$SET1_{Win}$ interactions. However, WDR5 is a more relevant target for drug discovery when immobilized onto the SPR sensor, where the free inhibitor in solution would better mimic *in vivo* function. This experimental design enables determinations of kinetic rate constants, contrasting the steady-state FP measurements. Our results also indicate that WDR5 did not undergo denaturation upon its immobilization onto the SPR sensor. In the future, it would be desirable to extend these kinetic studies to full-length $WRAD_2$ subunits, because of the suitability of these high-throughput approaches for examining long-lived protein–protein interactions. For instance, it would be interesting to conduct SPR measurements, in which a full-length SET1 subunit is immobilized on the chip surface and use WDR5 as an analyte in solution.

### Data Availability

All supporting data, materials, and sequence information are included within the main article and its Supplementary File.

*Biochemical Journal* (2021) **478** 2145–2161
https://doi.org/10.1042/BCJ20210253

## Competing Interests

The authors declare that there are no competing interests associated with the manuscript.

## Funding

This work was supported by the National Cancer Institute of the U.S. National Institutes of Health grant R01 CA140522 (to M.S.C.) and by the National Institute of General Medical Sciences of the U.S. National Institutes of Health grant R01 GM129429 (to L.M.).

## CRediT Author Contribution

**Liviu Movileanu:** Conceptualization, Resources, Supervision, Funding acquisition, Investigation, Writing — original draft, Project administration, Writing — review and editing. **Ali Imran:** Conceptualization, Data curation, Formal analysis, Validation, Investigation, Methodology, Writing — original draft, Writing — review and editing. **Brandon S. Moyer:** Conceptualization, Resources, Data curation, Validation, Investigation, Methodology, Writing — original draft, Writing — review and editing. **Ashley J. Canning:** Conceptualization, Data curation, Formal analysis, Validation, Investigation, Methodology. **Dan Kalina:** Conceptualization, Data curation, Formal analysis, Validation, Investigation, Methodology, Writing — review and editing. **Thomas M. Duncan:** Conceptualization, Supervision, Methodology. **Kelsey J. Moody:** Resources, Supervision, Funding acquisition, Project administration. **Aaron J. Wolfe:** Conceptualization, Resources, Supervision, Funding acquisition, Investigation, Project administration. **Michael S. Cosgrove:** Conceptualization, Resources, Supervision, Funding acquisition, Investigation, Writing — original draft, Project administration, Writing — review and editing.

## Acknowledgements

We are grateful to our colleagues in the Movileanu and Cosgrove laboratories and at Ichor Therapeutics Laboratories for their comments on the manuscript and stimulating discussions as well as for their assistance during the early stage of this project.

## Abbreviations

AUC, analytical ultracentrifugation; BLI, Biolayer Interferometry; FP, Fluorescence polarization anisotropy; H3K4, histone 3 lysine 4; ITC, isothermal titration calorimetry; $K_D$, the equilibrium dissociation constant; $K_{D\text{-}BLI}$, the equilibrium dissociation constant obtained by biolayer interferometry; $K_{D\text{-}FP}$, the equilibrium dissociation constant obtained by steady-state fluorescence polarization; $K_{D\text{-}SPR}$, the equilibrium dissociation constant obtained by surface plasmon resonance; KMT, lysine methyltransferases of histones; $k_{off}$, the dissociation rate constant; $k_{on}$, the association rate constant; MLL, Mixed lineage leukemia; MYC, transcription factor oncoprotein; PDPK1, 3-phosphoinositide-dependent protein kinase 1; PI3K, phosphatidylinositol 3-kinase; SET1, Suppressor of Variegation, Enhancer of Zeste, and Trithorax 1 lysine methyltransferases of histones; $SET1_{Win}$, 14-residue WDR5 interaction (Win) motif peptides of each SET1 protein; SPR, Surface plasmon resonance; WDR5, WD40 repeat protein 5; Win, evolutionarily conserved WDR5-interaction motif found in all SET1 family members; $WRAD_2$, subcomplex consisting of WDR5, retinoblastoma binding protein-5 (RbBP5), absent-small-homeotic-2-like protein (Ash2L), and dumpy-30 (DPY-30).

# References

1 Trievel, R.C. and Shilatifard, A. (2009) WDR5, a complexed protein. *Nat. Struct. Mol. Biol.* **16**, 678–680 https://doi.org/10.1038/nsmb0709-678
2 Crawford, B.D. and Hess, J.L. (2006) MLL core components give the green light to histone methylation. *ACS Chem. Biol.* **1**, 495–498 https://doi.org/10.1021/cb600367v
3 Cosgrove, M.S. and Patel, A. (2010) Mixed lineage leukemia: a structure-function perspective of the MLL1 protein. *FEBS J.* **277**, 1832–1842 https://doi.org/10.1111/j.1742-4658.2010.07609.x
4 Li, Y., Han, J., Zhang, Y., Cao, F., Liu, Z., Li, S. et al. (2016) Structural basis for activity regulation of MLL family methyltransferases. *Nature* **530**, 447–452 https://doi.org/10.1038/nature16952
5 Vedadi, M., Blazer, L., Eram, M.S., Barsyte-Lovejoy, D., Arrowsmith, C.H. and Hajian, T. (2017) Targeting human SET1/MLL family of proteins. *Protein Sci.* **26**, 662–676 https://doi.org/10.1002/pro.3129
6 Xue, H., Yao, T., Cao, M., Zhu, G., Li, Y., Yuan, G. et al. (2019) Structural basis of nucleosome recognition and modification by MLL methyltransferases. *Nature* **573**, 445–449 https://doi.org/10.1038/s41586-019-1528-1
7 Jiang, H. (2020) The complex activities of the SET1/MLL complex core subunits in development and disease. *Biochim. Biophys. Acta. Gene. Regul. Mech.* **1863**, 194560 https://doi.org/10.1016/j.bbagrm.2020.194560
8 Sha, L., Ayoub, A., Cho, U.S. and Dou, Y. (2020) Insights on the regulation of the MLL/SET1 family histone methyltransferases. *Biochim. Biophys. Acta Gene. Regul. Mech.* **1863**, 194561 https://doi.org/10.1016/j.bbagrm.2020.194561

9 Dou, Y., Milne, T.A., Ruthenburg, A.J., Lee, S., Lee, J.W., Verdine, G.L. et al. (2006) Regulation of MLL1 H3K4 methyltransferase activity by its core components. *Nat. Struct. Mol. Biol.* **13**, 713–719 https://doi.org/10.1038/nsmb1128
10 Lee, J.H., Tate, C.M., You, J.S. and Skalnik, D.G. (2007) Identification and characterization of the human Set1B histone H3-Lys4 methyltransferase complex. *J. Biol. Chem.* **282**, 13419–13428 https://doi.org/10.1074/jbc.M609809200
11 Patel, A., Dharmarajan, V., Vought, V.E. and Cosgrove, M.S. (2009) On the mechanism of multiple lysine methylation by the human mixed lineage leukemia protein-1 (MLL1) core complex. *J. Biol. Chem.* **284**, 24242–24256 https://doi.org/10.1074/jbc.M109.014498
12 Odho, Z., Southall, S.M. and Wilson, J.R. (2010) Characterization of a novel WDR5-binding site that recruits RbBP5 through a conserved motif to enhance methylation of histone H3 lysine 4 by mixed lineage leukemia protein-1. *J. Biol. Chem.* **285**, 32967–32976 https://doi.org/10.1074/jbc.M110.159921
13 Avdic, V., Zhang, P., Lanouette, S., Groulx, A., Tremblay, V., Brunzelle, J. et al. (2011) Structural and biochemical insights into MLL1 core complex assembly. *Structure* **19**, 101–108 https://doi.org/10.1016/j.str.2010.09.022
14 Patel, A., Vought, V.E., Dharmarajan, V. and Cosgrove, M.S. (2011) A novel non-SET domain multi-subunit methyltransferase required for sequential nucleosomal histone H3 methylation by the mixed lineage leukemia protein-1 (MLL1) core complex. *J. Biol. Chem.* **286**, 3359–3369 https://doi.org/10.1074/jbc.M110.174524
15 van Nuland, R., Smits, A.H., Pallaki, P., Jansen, P.W., Vermeulen, M. and Timmers, H.T. (2013) Quantitative dissection and stoichiometry determination of the human SET1/MLL histone methyltransferase complexes. *Mol. Cell Biol.* **33**, 2067–2077 https://doi.org/10.1128/MCB.01742-12
16 Zhang, P., Bergamin, E. and Couture, J.F. (2013) The many facets of MLL1 regulation. *Biopolymers* **99**, 136–145 https://doi.org/10.1002/bip.22126
17 Froimchuk, E., Jang, Y. and Ge, K. (2017) Histone H3 lysine 4 methyltransferase KMT2D. *Gene* **627**, 337–342 https://doi.org/10.1016/j.gene.2017.06.056
18 Ali, A. and Tyagi, S. (2017) Diverse roles of WDR5-RbBP5-ASH2L-DPY30 (WRAD) complex in the functions of the SET1 histone methyltransferase family. *J. Biosci.* **42**, 155–159 https://doi.org/10.1007/s12038-017-9666-9
19 Han, J., Li, T., Li, Y., Li, M., Wang, X., Peng, C. et al. (2019) The internal interaction in RBBP5 regulates assembly and activity of MLL1 methyltransferase complex. *Nucleic Acids Res.* **47**, 10426–10438 https://doi.org/10.1093/nar/gkz819
20 Kaustov, L., Lemak, A., Wu, H., Faini, M., Fan, L., Fang, X. et al. (2019) The MLL1 trimeric catalytic complex is a dynamic conformational ensemble stabilized by multiple weak interactions. *Nucleic Acids Res.* **47**, 9433–9447 https://doi.org/10.1093/nar/gkz697
21 Patel, A., Dharmarajan, V. and Cosgrove, M.S. (2008) Structure of WDR5 bound to mixed lineage leukemia protein-1 peptide. *J. Biol. Chem.* **283**, 32158–32161 https://doi.org/10.1074/jbc.C800164200
22 Patel, A., Vought, V.E., Dharmarajan, V. and Cosgrove, M.S. (2008) A conserved arginine-containing motif crucial for the assembly and enzymatic activity of the mixed lineage leukemia protein-1 core complex. *J. Biol. Chem.* **283**, 32162–32175 https://doi.org/10.1074/jbc.M806317200
23 Song, J.J. and Kingston, R.E. (2008) WDR5 interacts with mixed lineage leukemia (MLL) protein via the histone H3-binding pocket. *J. Biol. Chem.* **283**, 35258–35264 https://doi.org/10.1074/jbc.M806900200
24 Dharmarajan, V., Lee, J.H., Patel, A., Skalnik, D.G. and Cosgrove, M.S. (2012) Structural basis for WDR5 interaction (Win) motif recognition in human SET1 family histone methyltransferases. *J. Biol. Chem.* **287**, 27275–27289 https://doi.org/10.1074/jbc.M112.364125
25 Alicea-Velázquez, N.L., Shinsky, S.A., Loh, D.M., Lee, J.H., Skalnik, D.G. and Cosgrove, M.S. (2016) Targeted disruption of the interaction between WD-40 repeat protein 5 (WDR5) and mixed lineage leukemia (MLL)/SET1 family proteins specifically inhibits MLL1 and SETd1A methyltransferase complexes. *J. Biol. Chem.* **291**, 22357–22372 https://doi.org/10.1074/jbc.M116.752626
26 Shinsky, S.A., Monteith, K.E., Viggiano, S. and Cosgrove, M.S. (2015) Biochemical reconstitution and phylogenetic comparison of human SET1 family core complexes involved in histone methylation. *J. Biol. Chem.* **290**, 6361–6375 https://doi.org/10.1074/jbc.M114.627646
27 Stirnimann, C.U., Petsalaki, E., Russell, R.B. and Müller, C.W. (2010) WD40 proteins propel cellular networks. *Trends Biochem. Sci.* **35**, 565–574 https://doi.org/10.1016/j.tibs.2010.04.003
28 Santosh Kumar, H.S., Kumar, V., Pattar, S. and Telkar, S. (2016) Towards the construction of an interactome for Human WD40 protein family. *Bioinformation* **12**, 54–61 https://doi.org/10.6026/97320630012054
29 Jain, B.P. and Pandey, S. (2018) WD40 repeat proteins: signalling scaffold with diverse functions. *Protein J.* **37**, 391–406 https://doi.org/10.1007/s10930-018-9785-7
30 Ullius, A., Luscher-Firzlaff, J., Costa, I.G., Walsemann, G., Forst, A.H., Gusmao, E.G.et al. (2014) The interaction of MYC with the trithorax protein ASH2L promotes gene transcription by regulating H3K27 modification. *Nucleic Acids Res.* **42**, 6901–6920 https://doi.org/10.1093/nar/gku312
31 Thomas, L.R., Foshage, A.M., Weissmiller, A.M. and Tansey, W.P. (2015) The MYC-WDR5 nexus and cancer. *Cancer Res.* **75**, 4012–4015 https://doi.org/10.1158/0008-5472.CAN-15-1216
32 Thomas, L.R., Wang, Q., Grieb, B.C., Phan, J., Foshage, A.M., Sun, Q. et al. (2015) Interaction with WDR5 promotes target gene recognition and tumorigenesis by MYC. *Mol. Cell. Biochem.* **58**, 440–452 https://doi.org/10.1016/j.molcel.2015.02.028
33 Aho, E.R., Weissmiller, A.M., Fesik, S.W. and Tansey, W.P. (2019) Targeting WDR5: a WINning anti-cancer strategy? *Epigenet. Insights.* **12**, 2516865719865282 https://doi.org/10.1177/2516865719865282
34 Thomas, L.R., Adams, C.M., Wang, J., Weissmiller, A.M., Creighton, J., Lorey, S.L. et al. (2019) Interaction of the oncoprotein transcription factor MYC with its chromatin cofactor WDR5 is essential for tumor maintenance. *Proc. Natl Acad. Sci. U.S.A.* **116**, 25260–25268 https://doi.org/10.1073/pnas.1910391116
35 Thomas, L.R., Adams, C.M., Fesik, S.W., Eischen, C.M. and Tansey, W.P. (2020) Targeting MYC through WDR5. *Mol. Cell. Oncol.* **7**, 1709388 https://doi.org/10.1080/23723556.2019.1709388
36 Guarnaccia, A.D., Rose, K.L., Wang, J., Zhao, B., Popay, T.M., Wang, C.E. et al. (2021) Impact of WIN site inhibitor on the WDR5 interactome. *Cell Rep.* **34**, 108636 https://doi.org/10.1016/j.celrep.2020.108636
37 Downing, T.L., Soto, J., Morez, C., Houssin, T., Fritz, A., Yuan, F. et al. (2013) Biophysical regulation of epigenetic state and cell reprogramming. *Nat. Mater.* **12**, 1154–1162 https://doi.org/10.1038/nmat3777
38 Wang, P., Dreger, M., Madrazo, E., Williams, C.J., Samaniego, R., Hodson, N.W. et al. (2018) WDR5 modulates cell motility and morphology and controls nuclear changes induced by a 3D environment. *Proc. Natl Acad. Sci. U.S.A.* **115**, 8581–8586 https://doi.org/10.1073/pnas.1719405115
39 Guarnaccia, A.D. and Tansey, W.P. (2018) Moonlighting with WDR5: a cellular multitasker. *J. Clin. Med.* **7**, 21 https://doi.org/10.3390/jcm7020021

*Biochemical Journal* (2021) **478** 2145–2161
https://doi.org/10.1042/BCJ20210253


40 Bryan, A.F., Wang, J., Howard, G.C., Guarnaccia, A.D., Woodley, C.M., Aho, E.R. et al. (2020) WDR5 is a conserved regulator of protein synthesis gene expression. *Nucleic Acids Res.* **48**, 2924–2941 https://doi.org/10.1093/nar/gkaa051

41 Couture, J.F., Collazo, E. and Trievel, R.C. (2006) Molecular recognition of histone H3 by the WD40 protein WDR5. *Nat. Struct. Mol. Biol.* **13**, 698–703 https://doi.org/10.1038/nsmb1116

42 Han, Z., Guo, L., Wang, H., Shen, Y., Deng, X.W. and Chai, J. (2006) Structural basis for the specific recognition of methylated histone H3 lysine 4 by the WD-40 protein WDR5. *Mol. Cell* **22**, 137–144 https://doi.org/10.1016/j.molcel.2006.03.018

43 Schuetz, A., Allali-Hassani, A., Martín, F., Loppnau, P., Vedadi, M., Bochkarev, A. et al. (2006) Structural basis for molecular recognition and presentation of histone H3 by WDR5. *EMBO J.* **25**, 4245–4252 https://doi.org/10.1038/sj.emboj.7601316

44 Ruthenburg, A.J., Wang, W., Graybosch, D.M., Li, H., Allis, C.D., Patel, D.J. et al. (2006) Histone H3 recognition and presentation by the WDR5 module of the MLL1 complex. *Nat. Struct. Mol. Biol.* **13**, 704–712 https://doi.org/10.1038/nsmb1119

45 Avdic, V., Zhang, P., Lanouette, S., Voronova, A., Skerjanc, I. and Couture, J.F. (2011) Fine-tuning the stimulation of MLL1 methyltransferase activity by a histone H3-based peptide mimetic. *FASEB J.* **25**, 960–967 https://doi.org/10.1096/fj.10-171959

46 Iberg, A.N., Espejo, A., Cheng, D., Kim, D., Michaud-Levesque, J., Richard, S. et al. (2008) Arginine methylation of the histone H3 tail impedes effector binding. *J. Biol. Chem.* **283**, 3006–3010 https://doi.org/10.1074/jbc.C700192200

47 Ge, Z., Song, E.J., Kawasawa, Y.I., Li, J., Dovat, S. and Song, C. (2016) WDR5 high expression and its effect on tumorigenesis in leukemia. *Oncotarget* **7**, 37740–37754 https://doi.org/10.18632/oncotarget.9312

48 Sun, W., Guo, F. and Liu, M. (2018) Up-regulated WDR5 promotes gastric cancer formation by induced cyclin D1 expression. *J. Cell. Biochem.* **119**, 3304–3316 https://doi.org/10.1002/jcb.26491

49 Wang, F., Zhang, J., Ke, X., Peng, W., Zhao, G., Peng, S. et al. (2020) WDR5-Myc axis promotes the progression of glioblastoma and neuroblastoma by transcriptional activating CARM1. *Biochem. Biophys. Res. Commun.* **523**, 699–706 https://doi.org/10.1016/j.bbrc.2019.12.101

50 Karatas, H., Townsend, E.C., Bernard, D., Dou, Y. and Wang, S. (2010) Analysis of the binding of mixed lineage leukemia 1 (MLL1) and histone 3 peptides to WD repeat domain 5 (WDR5) for the design of inhibitors of the MLL1-WDR5 interaction. *J. Med. Chem.* **53**, 5179–5185 https://doi.org/10.1021/jm100139b

51 Karatas, H., Townsend, E.C., Cao, F., Chen, Y., Bernard, D., Liu, L. et al. (2013) High-affinity, small-molecule peptidomimetic inhibitors of MLL1/WDR5 protein-protein interaction. *J. Am. Chem. Soc.* **135**, 669–682 https://doi.org/10.1021/ja306028q

52 Senisterra, G., Wu, H., Allali-Hassani, A., Wasney, G.A., Barsyte-Lovejoy, D., Dombrovski, L. et al. (2013) Small-molecule inhibition of MLL activity by disruption of its interaction with WDR5. *Biochem. J.* **449**, 151–159 https://doi.org/10.1042/BJ20121280

53 Zhou, H., Liu, L., Huang, J., Bernard, D., Karatas, H., Navarro, A. et al. (2013) Structure-based design of high-affinity macrocyclic peptidomimetics to block the menin-mixed lineage leukemia 1 (MLL1) protein-protein interaction. *J. Med. Chem.* **56**, 1113–1123 https://doi.org/10.1021/jm3015298

54 Cao, F., Townsend, E.C., Karatas, H., Xu, J., Li, L., Lee, S. et al. (2014) Targeting MLL1 H3K4 methyltransferase activity in mixed-lineage leukemia. *Mol. Cell* **53**, 247–261 https://doi.org/10.1016/j.molcel.2013.12.001

55 Karatas, H., Li, Y., Liu, L., Ji, J., Lee, S., Chen, Y. et al. (2017) Discovery of a highly potent, cell-permeable macrocyclic peptidomimetic (MM-589) targeting the WD repeat domain 5 protein (WDR5)-mixed lineage leukemia (MLL) protein-protein interaction. *J. Med. Chem.* **60**, 4818–4839 https://doi.org/10.1021/acs.jmedchem.6b01796

56 Wang, F., Jeon, K.O., Salovich, J.M., Macdonald, J.D., Alvarado, J., Gogliotti, R.D. et al. (2018) Discovery of potent 2-Aryl-6,7-dihydro-5 H-pyrrolo[1,2-a]imidazoles as WDR5-WIN-site inhibitors using fragment-based methods and structure-based design. *J. Med. Chem.* **61**, 5623–5642 https://doi.org/10.1021/acs.jmedchem.8b00375

57 Aho, E.R., Wang, J., Gogliotti, R.D., Howard, G.C., Phan, J., Acharya, P. et al. (2019) Displacement of WDR5 from chromatin by a WIN site inhibitor with picomolar affinity. *Cell Rep.* **26**, 2916–2928.e2913 https://doi.org/10.1016/j.celrep.2019.02.047

58 Dennis, M.L., Morrow, B.J., Dolezal, O., Cuzzupe, A.N., Stupple, A.E., Newman, J. et al. (2019) Fragment screening for a protein-protein interaction inhibitor to WDR5. *Struct. Dyn.* **6**, 064701 https://doi.org/10.1063/1.5122849

59 Tian, J., Teuscher, K.B., Aho, E.R., Alvarado, J.R., Mills, J.J., Meyers, K.M. et al. (2020) Discovery and structure-based optimization of potent and selective WD repeat domain 5 (WDR5) inhibitors containing a dihydroisoquinolinone bicyclic core. *J. Med. Chem.* **63**, 656–675 https://doi.org/10.1021/acs.jmedchem.9b01608

60 Bolshan, Y., Getlik, M., Kuznetsova, E., Wasney, G.A., Hajian, T., Poda, G. et al. (2013) Synthesis, optimization, and evaluation of novel small molecules as antagonists of WDR5-MLL interaction. *ACS Med. Chem. Lett.* **4**, 353–357 https://doi.org/10.1021/ml300467n

61 Getlik, M., Smil, D., Zepeda-Velázquez, C., Bolshan, Y., Poda, G., Wu, H. et al. (2016) Structure-based optimization of a small molecule antagonist of the interaction between WD repeat-containing protein 5 (WDR5) and mixed-lineage leukemia 1 (MLL1). *J. Med. Chem.* **59**, 2478–2496 https://doi.org/10.1021/acs.jmedchem.5b01630

62 Schapira, M. and Arrowsmith, C.H. (2016) Methyltransferase inhibitors for modulation of the epigenome and beyond. *Curr. Opin. Chem .Biol.* **33**, 81–87 https://doi.org/10.1016/j.cbpa.2016.05.030

63 Schapira, M., Tyers, M., Torrent, M. and Arrowsmith, C.H. (2017) WD40 repeat domain proteins: a novel target class? *Nat. Rev. Drug Discov.* **16**, 773–786 https://doi.org/10.1038/nrd.2017.179

64 Gupta, A., Xu, J., Lee, S., Tsai, S.T., Zhou, B., Kurosawa, K. et al. (2018) Facile target validation in an animal model with intracellularly expressed monobodies. *Nat. Chem. Biol.* **14**, 895–900 https://doi.org/10.1038/s41589-018-0099-z

65 Zhang, P., Lee, H., Brunzelle, J.S. and Couture, J.F. (2012) The plasticity of WDR5 peptide-binding cleft enables the binding of the SET1 family of histone methyltransferases. *Nucleic Acids Res.* **40**, 4237–4246 https://doi.org/10.1093/nar/gkr1235

66 Wu, X.H., Chen, R.C., Gao, Y. and Wu, Y.D. (2010) The effect of Asp-His-Ser/Thr-Trp tetrad on the thermostability of WD40-repeat proteins. *Biochemistry* **49**, 10237–10245 https://doi.org/10.1021/bi101321y

67 Xu, C. and Min, J. (2011) Structure and function of WD40 domain proteins. *Protein Cell* **2**, 202–214 https://doi.org/10.1007/s13238-011-1018-1

68 Denesyuk, A., Denessiouk, K. and Johnson, M.S. (2018) Top surface blade residues and the central channel water molecules are conserved in every repeat of the integrin-like β-propeller structures. *J. Struct. Biol.* **201**, 155–161 https://doi.org/10.1016/j.jsb.2017.10.005

69 Shinsky, S.A., Hu, M., Vought, V.E., Ng, S.B., Bamshad, M.J., Shendure, J. et al. (2014) A non-active-site SET domain surface crucial for the interaction of MLL1 and the RbBP5/Ash2L heterodimer within MLL family core complexes. *J. Mol. Biol.* **426**, 2283–2299 https://doi.org/10.1016/j.jmb.2014.03.011

70 Shinsky, S.A. and Cosgrove, M.S. (2015) Unique role of the WD-40 repeat protein 5 (WDR5) subunit within the mixed lineage leukemia 3 (MLL3) histone methyltransferase complex. *J. Biol. Chem.* **290**, 25819–25833 https://doi.org/10.1074/jbc.M115.684142
71 Weeramange, C.J., Fairlamb, M.S., Singh, D., Fenton, A.W. and Swint-Kruse, L. (2020) The strengths and limitations of using biolayer interferometry to monitor equilibrium titrations of biomolecules. *Protein Sci.* **29**, 1018–1034 https://doi.org/10.1002/pro.3827
72 Concepcion, J., Witte, K., Wartchow, C., Choo, S., Yao, D., Persson, H. et al. (2009) Label-free detection of biomolecular interactions using bioLayer interferometry for kinetic characterization. *Comb. Chem. High Throughput Screen.* **12**, 791–800 https://doi.org/10.2174/138620709789104915
73 Shah, N.B. and Duncan, T.M. (2014) Bio-layer interferometry for measuring kinetics of protein-protein interactions and allosteric ligand effects. *J. Vis. Exp.* **84**, e51383 https://doi.org/10.3791/51383
74 Movileanu, L., Cheley, S., Howorka, S., Braha, O. and Bayley, H. (2001) Location of a constriction in the lumen of a transmembrane pore by targeted covalent attachment of polymer molecules. *J. Gen. Physiol.* **117**, 239–251 https://doi.org/10.1085/jgp.117.3.239
75 Wolfe, A.J., Gugel, J.F., Chen, M. and Movileanu, L. (2018) Kinetics of membrane protein-detergent interactions depend on protein electrostatics. *J. Phys. Chem. B* **122**, 9471–9481 https://doi.org/10.1021/acs.jpcb.8b07889
76 Jarmoskaite, I., AlSadhan, I., Vaidyanathan, P.P. and Herschlag, D. (2020) How to measure and evaluate binding affinities. *eLife* **9**, e57264 https://doi.org/10.7554/eLife.57264
77 Boozer, C., Kim, G., Cong, S., Guan, H. and Londergan, T. (2006) Looking towards label-free biomolecular interaction analysis in a high-throughput format: a review of new surface plasmon resonance technologies. *Curr. Opin. Biotechnol.* **17**, 400–405 https://doi.org/10.1016/j.copbio.2006.06.012
78 Masson, J.F. (2017) Surface plasmon resonance clinical biosensors for medical diagnostics. *ACS Sens.* **2**, 16–30 https://doi.org/10.1021/acssensors.6b00763
79 Drescher, D.G., Selvakumar, D. and Drescher, M.J. (2018) Analysis of protein interactions by surface plasmon resonance. *Adv. Protein Chem. Struct. Biol.* **110**, 1–30 https://doi.org/10.1016/bs.apcsb.2017.07.003
80 Wolfe, A.J., Si, W., Zhang, Z., Blanden, A.R., Hsueh, Y.C., Gugel, J.F. et al. (2017) Quantification of membrane protein-detergent complex interactions. *J. Phys. Chem. B* **121**, 10228–10241 https://doi.org/10.1021/acs.jpcb.7b08045
81 Wolfe, A.J., Hsueh, Y.C., Blanden, A.R., Mohammad, M.M., Pham, B., Thakur, A.K. et al. (2017) Interrogating detergent desolvation of nanopore-forming proteins by fluorescence polarization spectroscopy. *Anal. Chem.* **89**, 8013–8020 https://doi.org/10.1021/acs.analchem.7b01339
82 Rossi, A.M. and Taylor, C.W. (2011) Analysis of protein-ligand interactions by fluorescence polarization. *Nat. Protoc.* **6**, 365–387 https://doi.org/10.1038/nprot.2011.305
83 Wolfe, A.J., Gugel, J.F., Chen, M. and Movileanu, L. (2018) Detergent desorption of membrane proteins exhibits two kinetic phases. *J. Phys. Chem. Lett.* **9**, 1913–1919 https://doi.org/10.1021/acs.jpclett.8b00549
84 Tolkatchev, D., Xu, P. and Ni, F. (2003) Probing the kinetic landscape of transient peptide-protein interactions by use of peptide (15)n NMR relaxation dispersion spectroscopy: binding of an antithrombin peptide to human prothrombin. *J. Am. Chem. Soc.* **125**, 12432–12442 https://doi.org/10.1021/ja021238l
85 Gianni, S., Engström, A., Larsson, M., Calosci, N., Malatesta, F., Eklund, L. et al. (2005) The kinetics of PDZ domain-ligand interactions and implications for the binding mechanism. *J. Biol. Chem.* **280**, 34805–34812 https://doi.org/10.1074/jbc.M506017200
86 Eildal, J.N., Hultqvist, G., Balle, T., Stuhr-Hansen, N., Padrah, S., Gianni, S. et al. (2013) Probing the role of backbone hydrogen bonds in protein-peptide interactions by amide-to-ester mutations. *J. Am. Chem. Soc.* **135**, 12998–13007 https://doi.org/10.1021/ja402875h
87 Paul, F., Wehmeyer, C., Abualrous, E.T., Wu, H., Crabtree, M.D., Schöneberg, J. et al. (2017) Protein-peptide association kinetics beyond the seconds timescale from atomistic simulations. *Nat. Commun.* **8**, 1095 https://doi.org/10.1038/s41467-017-01163-6
88 Stadmiller, S.S., Aguilar, J.S., Parnham, S. and Pielak, G.J. (2020) Protein-peptide binding energetics under crowded conditions. *J. Phys. Chem. B* **124**, 9297–9309 https://doi.org/10.1021/acs.jpcb.0c05578
89 Mohammad, M.M. and Movileanu, L. (2008) Excursion of a single polypeptide into a protein pore: simple physics, but complicated biology. *Eur. Biophys. J.* **37**, 913–925 https://doi.org/10.1007/s00249-008-0309-9
90 Bikwemu, R., Wolfe, A.J., Xing, X. and Movileanu, L. (2010) Facilitated translocation of polypeptides through a single nanopore. *J. Phys. Condens. Matter.* **22**, 454117 https://doi.org/10.1088/0953-8984/22/45/454117
91 Qin, S., Pang, X. and Zhou, H.X. (2011) Automated prediction of protein association rate constants. *Structure* **19**, 1744–1751 https://doi.org/10.1016/j.str.2011.10.015
92 Alsallaq, R. and Zhou, H.X. (2008) Electrostatic rate enhancement and transient complex of protein-protein association. *Proteins* **71**, 320–335 https://doi.org/10.1002/prot.21679
93 Qin, S. and Zhou, H.X. (2013) PI(2)PE: a suite of web servers for predictions ranging from protein structure to binding kinetics. *Biophys. Rev.* **5**, 41–46 https://doi.org/10.1007/s12551-012-0086-7
94 Zhou, H.X. (2010) Rate theories for biologists. *Q. Rev. Biophys.* **43**, 219–293 https://doi.org/10.1017/S0033583510000120
95 Pang, X. and Zhou, H.X. (2017) Rate constants and mechanisms of protein-ligand binding. *Annu. Rev. Biophys.* **46**, 105–130 https://doi.org/10.1146/annurev-biophys-070816-033639